IEEE Access
Multidisciplinary | Rapid Review | Open Access Journal

Received July 31, 2019, accepted August 19, 2019, date of publication August 22, 2019, date of current version September 5, 2019.

Digital Object Identifier 10.1109/ACCESS.2019.2936879

A New Adaptive High-Order Unscented Kalman Filter for Improving the Accuracy and Robustness of Target Tracking

WEIDONG ZHOU AND JIAXIN HOU, (Student Member, IEEE)
Department of Automation, Harbin Engineering University, Harbin 150001, China
Corresponding author: Jiaxin Hou (houjiaxin@hrbeu.edu.cn)

This work was supported by the National Natural Science Foundation of China under Grant 61573113 and Grant 61371173.

ABSTRACT In target tracking, the tracking process needs to constantly update the data information. For maneuvering target, model mismatch and loss of high-order moment information disrupt the accuracy of the state estimation. In this paper, an adaptive high-order unscented Kalman filter (AHUKF) algorithm is proposed for the case of errors occurring in the capturing of model dynamic behavior using the classical unscented Kalman filter (UKF) algorithm. By introducing the free parameter, the analytical solution of the high-order unscented transformation (UT) was obtained, the basis for choosing free parameters was analyzed, and the stability of the algorithm was discussed. A method for obtaining the optimal adaptive factor based on the prediction residual estimation covariance matrix was proposed, which reduces the influence of the dynamic model error and was applied to the target tracking model. In this paper, the proposed AHUKF is applied to a target tracking problem with state mutation, different sampling intervals, and different turn rates, respectively. Simulation results for target tracking illustrate that the proposed algorithm is more accurate and robust than the UKF, high-order unscented Kalman filter (HUKF) and adaptive unscented Kalman filter (AUKF).

INDEX TERMS UKF, optimal adaptive factor, adaptive filtering, orthogonality principle, high-order UT sampling.

I. INTRODUCTION

In recent years, the study of dynamic systems has been widely used in different fields. Nonlinear filtering is an advantageous method used to deal with dynamic systems, which plays an important role in target tracking, integrated navigation, positioning, control, and signal processing [1]–[8]. Since there is no closed analytical solution for solving nonlinear problems, nonlinear filtering has been committed to making a lot of effort to solve the nonlinear state estimation problem by function approximation and deterministic sampling method of approximate nonlinear distribution [9]. The most typical method is the extended Kalman filter (EKF) [10], [11]. Even though EKF has been used widely, it has several deficiencies including crude approximations, and it may experience divergence when the filtering problem exhibits highly non-linear characteristics [12]. So, EKF is a suboptimal filter [13], [14]. Other nonlinear transformation methods mainly include the unscented Kalman filter (UKF) [15]–[17], cubature Kalman filter (CKF) [17], [18], and central difference Kalman filter (CDKF) [19], there are classified within the range of sigma points filters (SPFs).

Different rules are used to select sampling points and corresponding weights, and the posterior mean and covariance of the state of the nonlinear system are satisfied. Whatever the degree of nonlinearity, SPFs can approach the posterior mean and covariance of any nonlinear system at least with second-order Taylor accuracy. In addition, SPFs don't need to calculate the Jacobian matrix in the filtering process, so SPFs reduce the number of tedious calculations and are easier to implement than the EKF [20], [21] and the nonlinear function is also not required to be continuously differentiable, which effectively overcomes the limitation of the EKF [22]. In addition, many experts have seen a surge of research interest on the H_∞ filtering problems for nonlinear systems, while the H_∞ theory can be utilized in the occasion when the disturbances are assumed to have bounded energy [23]–[25].

The associate editor coordinating the review of this article and approving it for publication was Lifeng Ma.

This work is licensed under a Creative Commons Attribution 4.0 License. For more information, see http://creativecommons.org/licenses/by/4.0/

Within the category of SPFs, the UKF uses $2n + 1$ sigma points and the unscented transform (UT) to propagate the mean value and (cross) covariance through nonlinear mapping using the same sampling points as system state distribution. The UT is a statistical linear regression (SLR), whose regression coefficient matrix can be regarded as the meaningful approximation of the Jacobian matrix, eliminating the tedious derivation and calculation of the Jacobian/Hessian matrix and approximates the mean value and covariance of the original distribution of the state. The UKF based on the UT is far better than the standard EKF in extensive applications [9], [26]. When compared with the particle filter [27], the UKF has lower computational requirements [28], [29]. The CKF can be regarded as a special form of UKF [15], [16]. Although H_∞ filter performs well when the prior information is unknown, however, H_∞ filtering cannot guarantee the minimum variance of estimation error or the variation is within a certain range [23]–[25].

UKF is usually better than the other filters in computational complexity and performance. Therefore, the UKF was accuracy chosen as a typical nonlinear Gaussian filter to be studied in this paper.

Considerable improvements have been made on the development of UKF. In reference [30], the concept of maximum a posterior and the random weighting criterion are used to establish the noise statistics data and present a new a maximum posterior and random weighting based adaptive UKF (MRAUKF). The noise statistics of the system are estimated and adjusted online, and applied to the navigation system. MRAUKF has a great advantage over the classical UKF in the case of uncertain system noise. However, for state mutations with the large impulse response, its filtering convergence is poor. A nonlinear filtering algorithm based on UKF for event triggering data transmission and packet loss in nonlinear dynamic systems is proposed and applied to wireless sensor networks, the prediction error covariance is bounded and convergent, and a sufficient condition for the random stability of the filter is obtained [31]. However, for motion vehicles with a large run rate, the filtering effect is poor.

A third-order UKF and a robust third-order UKF are proposed for the state estimation of nonlinear systems with unknown inputs, and the detailed derivation of the filter is given. The computational cost is increased relatively, and the accuracy is improved [32]. However, there is little advantage in the higher dimensional states. In references [33]–[35], the Huber-M estimation method is used to improve the robustness of UKF, by minimizing a Huber cost function that is a combined and norm. However, the influence function of Huber will not be reduced, which may reduce the estimation performance of the filtering algorithm [36]–[39]. The emergence of a marginalized UKF method is applied to the field of target tracking and integrated navigation. The algorithm only uses a few sampling points to estimate the deviation of the inertial sensors, reducing the computational complexity. However, the ability of sigma points to capture high-order moment information is limited, so the accuracy is difficult to guarantee [40], [41].

The above algorithm has been improved to some extent, but there are still limitations. When the filter is stable, the UKF loses the ability to track the abrupt state and the strong maneuvering target. This is due to the poor robustness of the UKF when the system model is uncertain, decreasing the estimation accuracy.

To further improve the robustness of the filter in the case of model mismatch. Xiong et al. designed the robust extended Kalman Filter (REKF) to ensure that the sufficient conditions for the filter stability could be fulfilled. Further, automatically adjust the error covariance matrix in response to the external environment interference [42]. However, because of the inherent defects of EKF, adaptive REKF is not feasible in real-time. References [43] and [44] apply the adaptive estimation algorithm to the current statistical (CS) model for the square-root CKF (SCKF) without free parameters, but when the system has a large mutation or model mismatch $C_{k+1} < 1$, the algorithm would fail. An adaptive-horizon iterative unbiased finite impulse response (UFIR) filter was proposed, and the author applied a real-time N_{opt} estimation strategy. Zhao *et al.* present the concepted of the maximum allowed horizon and allows the selection of a target horizon in a single iteration cycle and the design of adaptive horizon UFIR (AUFIR) [45]. However, for time-varying systems, the choice of N_{opt} is complex and difficult to determine quickly. Wang proposed an adaptive robust UKF (ARUKF), which reduces system model uncertainty. However, the adaptive and the equivalent weighting factors are determined by empirical evidence in ARUKF, this method fails to fundamentally solve the limitations of UKF [46].

Based on the above mentioned methods, the robustness of the algorithm is improved to some extent. However, these methods only improve the accuracy of general algorithms on the basis of second-order accuracy. In theory, the higher the order of the filter, the more the higher order moment information be captured, and the higher the filter accuracy. UKF is essentially a nonlinear filtering method based on second-order UT, which can only match the second-order moment of Taylor series expansion of nonlinear functions, so the error is limited, and the accuracy needs to be improved.

In recent years, high-order filters have been presented continuously, such as the fourth order unscented filter [47], fifth order UKF [9], and a skewed unscented Kalman filter [48], which achieve higher accuracy than the traditional second-order filter. However, the above mentioned high-order methods don't have an analytic solution and fail to complete the selection of sigma points and weights of high-order UT changes, thus they cannot constitute as a high-order UKF. Ponomareva et al. is proposed which generates sample points and corresponding probability weights that match exactly the predicted values of average marginal skewness and average marginal kurtosis of the unobserved state variables [49]. However, the free parameter is not defined in the UKF, so it is not a high-order UT in the true sense.

In this paper, a new adaptive high-order UKF is proposed. Based on a high-order UT form, through a high-order approximation, more deterministic sampling points and a more reasonable distribution are obtained. This distribution was used to match the probability distribution of the state to obtain the high-order UKF form. Then the error truncation was kept above the fourth order moment. The high-order sigma points were produced by using the high-order UT to improve the filtering accuracy of the UKF. When the filtering effect was optimal, the gain matrix remained stationary. As the system encountered a strong nonlinear condition or the model mutation, the gain matrix struggled to keep up with the required values of the system. The error covariance of state posterior estimation was seriously inconsistent with the true covariance matching degree, which led to the difficulty of the system convergence and even the failure of filtering. The accuracy improvements also depend on the matching degree of covariance. To solve this problem, an adaptive adjustment factor based on the residual vector was introduced to reduce the weight of covariance of a filter in the stationary state and to further adjust the influence of the gain matrix on the system. The effect of state mutations and strong nonlinearity on the filtering performance was suppressed, and the ill-conditioned covariance was avoided to affect the performance and robustness of the filter.

The key contributions of this paper are expressed as follows: First of all, the defects of standard UKF sigma points sampling method are analyzed, a high-order sampling strategy is proposed to match the probability distribution of the state to improve the accuracy of target tracking. Furthermore, according to the principle of orthogonality and the principle of minimum variance, the optimal adaptive factor is derived, reduce the error caused by the mismatch of the dynamic model, the adaptive ability and robustness of the algorithm are further improved in the whole filtering process. The stability of the proposed AHUKF algorithm is discussed, and the rationality of selecting free parameters is proved. Finally, we verify the superiority of AHUKF under different models and conditions.

The organization of this paper proceeds as follows: Introduce the UKF algorithm model and the sources of error were analyzed in Section II. In Section III, intuitively describe the sigma points selection strategy, and improved of UKF algorithm and discussed on the stability of algorithm. In Section IV, simulation results for the target tracking problem with different models are then presented, to compare the performance of the proposed AHUKF and the existing filter. Finally, we draw conclusions and presented future research work in Section V.

II. UKF ALGORITHM MODEL AND DEFICIENCY

Consider the following discrete-time nonlinear stochastic system as represented by the state-space model [50], [51]:

$$\begin{cases} x_k = f_{k-1}\left(x_{k-1}\right) + w_{k-1} \\ z_k = h_k\left(x_k\right) + v_k \end{cases} \tag{1}$$

where $x_k \in \mathbb{R}^n$ and $z_k \in \mathbb{R}^m$ denote the state vector and measurement vector, respectively, with corresponding dimensions. $f(\cdot)$ and $h(\cdot)$ are any known functions, that denote the nonlinear dynamic model function and measurement model function, respectively, with corresponding dimensions. $w_k \in \mathbb{R}^n$ and $v_k \in \mathbb{R}^n$ are respectively Gaussian process and measurement noise vectors with zero mean vectors and covariance matrices Q_k and R_k. k is the discrete time. The following statistical characteristics are used:

$$\begin{cases} E\left[w_k\right] = 0 & \operatorname{cov}\left(w_k, w_j\right) = Q_k \delta_{kj} \\ E\left[v_k\right] = 0 & \operatorname{cov}\left(v_k, v_j\right) = R_k \delta_{kj} \\ \operatorname{cov}\left(w_k, v_j\right) = 0 & \end{cases} \tag{2}$$

where Q_k and R_k are positive definite matrices, with corresponding dimensions. δ_{kj} is the $Kroneker - \delta$ function. The classical UKF filtering algorithm for nonlinear systems is as follows:

Initialization:

$$\begin{cases} \hat{x}_0 = E\left[x_0\right] \\ P_0 = E\left[\left(x_0 - \hat{x}_0\right)\left(x_0 - \hat{x}_0\right)^T\right] \end{cases} \tag{3}$$

Sigma points calculation:

$$\begin{cases} \xi_{k-1}^i = \hat{x}_{k-1}, & i = 0 \\ \xi_{k-1}^i = \hat{x}_{k-1} + (\sqrt{(n+\kappa)P_{k-1}})_i, & i = 1 \sim n \\ \xi_{k-1}^i = \hat{x}_{k-1} - (\sqrt{(n+\kappa)P_{k-1}})_i, & i = n+1 \sim 2n \end{cases} \tag{4}$$

$$\begin{cases} \omega_c^0 = \dfrac{\kappa}{n+\kappa} \\ [6pt]\omega_m^0 = \dfrac{\kappa}{n+\kappa} + \left(1 - \alpha^2 + \beta\right) \\ \omega_c^i = \omega_m^i = \dfrac{\kappa}{2(n+\kappa)}, \quad i = 1 \sim 2n \end{cases} \tag{5}$$

where $\kappa = 3 - n$ is a scaling free parameter, n is the state dimension with different models. α is usually set to $1e-4 \le \alpha \le 1$. i denotes the ith sampling points and $(\sqrt{(n+\kappa)P})_i$ denotes the ith column of the square root of the matrix $(n+\kappa)P$. $\beta \ge 0$ denotes a parameter that is to be selected and is a non-negative weight coefficient. $\beta \ge 0$ can combine the dynamic difference of the high-order in the equation.

A. TIME UPDATE

$$\xi_{k|k-1}^i = f\left(\xi_{k-1}^i\right), \quad i = 0 \sim 2n \tag{6}$$

$$\hat{x}_{k|k-1} = \sum_{i=0}^{2n} \omega_m^i \xi_{k|k-1}^i \tag{7}$$

$$P_{k|k-1} = \sum_{i=0}^{2n} \omega_c^i (\xi_{k|k-1}^i - \hat{x}_{k|k-1}^i)(\xi_{k|k-1}^i - \hat{x}_{k|k-1}^i)^T + Q_k \tag{8}$$

B. MEASUREMENT UPDATE

$$\begin{cases} \xi_{k|k-1}^{\prime i} = \hat{x}_{k|k-1}, & i = 0 \\ \xi_{k|k-1}^{\prime i} = \hat{x}_{k|k-1} + (\sqrt{(n+\kappa)P_{k|k-1}})_i, & i = 1 \sim n \\ \xi_{k|k-1}^{\prime i} = \hat{x}_{k|k-1} - (\sqrt{(n+\kappa)P_{k|k-1}})_i, & i = n+1 \sim 2n \end{cases} \tag{9}$$

$$\gamma^i_{k|k-1} = h(\xi'^i_{k|k-1}) \tag{10}$$

$$\hat{z}_{k|k-1} = \sum_{i=0}^{2n} \omega^i_m \gamma^i_{k|k-1} \tag{11}$$

$$P^{zz}_{k|k-1} = \sum_{i=0}^{2n} \omega^i_c (\gamma^i_{k|k-1} - \hat{z}_{k|k-1}(\gamma^i_{k|k-1} - \hat{z}_{k|k-1})^T + R_k \tag{12}$$

$$P^{xz}_{k|k-1} = \sum_{i=0}^{2n} \omega^i_c (\xi^i_{k|k-1} - \hat{x}^i_{k|k-1})(\gamma^i_{k|k-1} - \hat{z}_{k|k-1})^T \tag{13}$$

$$K_k = P^{xz}_{k|k-1}(P^{zz}_{k|k-1})^{-1} \tag{14}$$

$$\hat{x}_{k|k} = \hat{x}_{k|k-1} + K_k(z_k - \hat{z}_{k|k-1}) \tag{15}$$

$$P_{k|k} = P_{k|k-1} - K_k P^{zz}_{k|k-1} K^T_k \tag{16}$$

According to the linear minimum variance estimation criterion [52], [53], the estimation accuracy of UKF depends entirely on the calculations of mean and covariance in equations (7), (8) and (11)-(13), when the measurement is updated. Since the system is non-linear, the linear minimum variance estimation cannot represent the Gaussian distribution by means of mean and covariance, and cannot obtain the optimal state estimation output. Note that the state posterior estimation error increases with the sampling interval. When the system reaches a stationary state, the gain matrix in equation (14) reaches a constant value. As mutation or strong nonlinearity of the system occurs and the target is maneuvering at a high turn rate, the gain matrix is difficult to reach the required value of the system in the first moment. UKF fails to capture high-order moment information, and its adaptability to system mutation is also poor. Through the analysis of nonlinear UKF frame, the accurate calculation of covariance cannot be ignored. Therefore, this paper started with the mean and covariance of UKF, by matching high-order moment information, and introduced adaptive factor to modify predictive covariance to improve the filtering accuracy and robustness.

III. IMPROVED UKF ALGORITHM

The mean and covariance of the sample points to be estimated are obtained by non-linear function transformations and the ability of these samples to cover the entire probability distribution is directly determined by the selection strategy of the sigma points. The ability of the sigma points to match the order moment information is proportional to the accuracy. In classical UKF, equations (4) and (9) represent the selection of $2n + 1$ sigma points. The mean and covariance of the sample points to be estimated are obtained by non-linear function transformations and the ability of these samples to cover the entire probability distribution is directly determined by the selection strategy of the sigma points. The ability of the sigma points to match the order moment information is proportional to the accuracy. In classical UKF, equations (4) and (9) represent the selection of $2n + 1$ sigma points. This set of sigma points can match the information of the first two moments (mean and covariance) of random variables and maintain symmetry. In Fig. 1 gives the sigma points sampling strategy of UT in the second order case. The number of central sigma points and symmetric sigma points are 1 and $2n$, respectively.

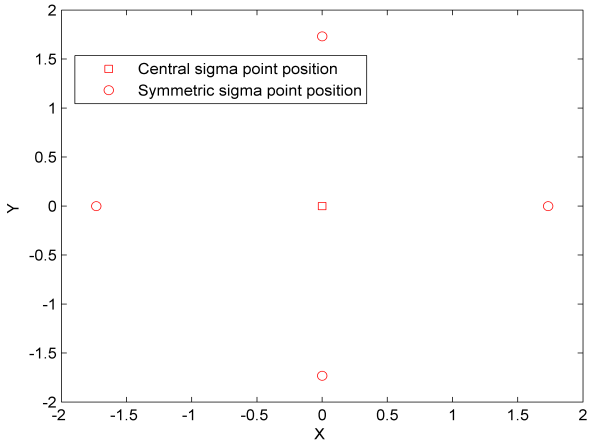

FIGURE 1. Standard UT sigma points.

Through the above analysis, the standard UT only perfectly matches the first two moments (mean and covariance). When the skewness and kurtosis of a random variable have a serious effect on the probability distribution, the sigma points obtained by the standard UT mismatch the statistical characteristics of the prior probability distribution well, which leads to underestimation. Therefore, to keep the accuracy of first and second moments and to match the third and fourth moments, a high-order UT was introduced in this paper, and the derivation process of high-order the UKF was obtained, thus improving the accuracy of the UKF. To reduce the influence of the dynamic model error, an adaptive filter based on the predictive residual estimation covariance matrix was proposed to improve the accuracy of model mismatch of state estimation when the target systematic mutation and maneuvers at high turn rate.

A. HIGH-ORDER SIGMA SAMPLING STRATEGY

The implementation of a high-order UKF requires the technical support of a high order UT. Sigma points cover the information of high-order moments of random variables as much as possible, including mean, variance, skewness, and kurtosis. The high-order UT needs to select a set of sigma points $2n^2 + 1$.

To accurately match the first four moments of the standard Gaussian random variables, the sigma points of high-order UT and the corresponding weights must satisfy the following conditions and be divided into three kinds of sigma points [54]:

$$\left\{ \begin{array}{l} \omega_0 + 2n\omega_1 + 2n(n-1)\omega_2 - 1 \\ 2\omega_1 s_1^2 + 4(n-1)\omega_2 s_2^2 - 1 \\ 2\omega_1 s_1^4 + 4(n-1)\omega_2 s_2^4 - 3 \\ 4\omega_2 s_2^4 - 1 \end{array} \right\} = 0 \tag{17}$$

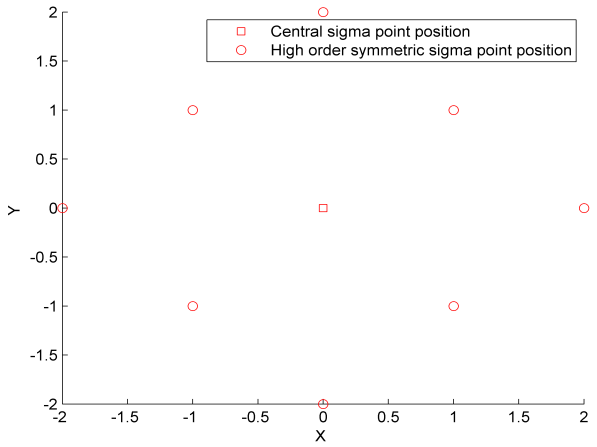

FIGURE 2. High-order UT sigma points.

where ω_0 is the weight of the central symmetry points. s_1 and ω_1 denote the position and weight of symmetric sigma points, respectively. s_2 and ω_2 denote the position and weight of the high-order symmetric sigma points, respectively.

The sigma points and weights are calculated in the following:

Calculation of sigma point and weight of the first kind:

$$\begin{cases} \xi^{i0}_{k|k-1} = \hat{x}_{k-1} \\ \omega_0 = \dfrac{-2n^2 + (4-2n)\kappa^2 + (4\kappa+4)n}{(n+\kappa)^2(4-n)} \end{cases} \tag{18}$$

Calculation of sigma point and weight of the second kind:

$$\begin{cases} \xi^{i1}_{k|k-1} = \hat{x}_{k-1} \pm \sqrt{\dfrac{(4-n)(n+\kappa)}{(\kappa+2-n)}} P_{k-1} e_{i1} \\ \omega_1 = \dfrac{(\kappa+2-n)^2}{2(n+\kappa)^2(4-n)} \quad i_1 = 1, 2, \cdots, n \end{cases} \tag{19}$$

Calculation of sigma point and weight of the third kind:

$$\begin{cases} \xi^{i2}_{k|k-1} = \hat{x}_{k-1} \pm \sqrt{(n+\kappa) P_{k-1}} e^{+}_{i2} \\ \xi^{i2}_{k|k-1} = \hat{x}_{k-1} \pm \sqrt{(n+\kappa) P_{k-1}} e^{-}_{i2} \\ \omega_2 = \frac{1}{(n+\kappa)^2} \quad i_2 = 1, 2, \cdots 0.5n(n-1) \end{cases} \tag{20}$$

where e_{i1}, e^{+}_{i2} and e^{-}_{i2} satisfy the following expressions:

$$e_{i1} = [0, \cdots 0, 1, 0, \cdots 0] \tag{21}$$

$$e^{+}_{i2} = \sqrt{\frac{1}{2}} (e_k + e_l) : k < l, \quad k, l = 1, 2 \cdots n \tag{22}$$

$$e^{-}_{i2} = \sqrt{\frac{1}{2}} (e_k - e_l) : k < l, \quad k, l = 1, 2 \cdots n \tag{23}$$

In Fig. 2, it is shown that the high-order UKF of 2-Dimensional systems uses symmetric sigma sampling strategy to complete the high-order moment information matching for random variables.

Combined with Fig. 2 and the equations (18)-(20), the first kind of sigma point is located in the center, and the number of them is 1. The second kind of sigma point is located at s_1 from the center point, and the corresponding number is $2n$. The third kind of sigma point is at s_2 and the corresponding number is $2n(n-1)$.

Let $\omega_2 = \frac{1}{(n+\kappa)^2}$, then $s_1 = \sqrt{\frac{(4-n)(n+\kappa)}{(\kappa+2-n)}}$, and $s_2 = \sqrt{\frac{(n+\kappa)}{2}}$. The state dimensions $n = 4$ and $n \neq 4$ are discussed by analogy with the standard UT, the analytic solution of the equation is obtained, and the position of sigma points and the corresponding weights s_1, s_2, ω_1 and $\omega_2$are obtained.

When, $n = 4$ the corresponding sigma points and weights are calculated by the above equations (18)-(20). When, let, the analytic solution of equation (17) is obtained.

The corresponding expression is as follows:

$$\begin{cases} \omega_0 = \dfrac{2}{n+2} \; \omega_1 = \dfrac{(4-n)}{2(n+2)^2} \; \omega_2 = \dfrac{2}{(n+2)^2} \\ s_1 = \sqrt{n+2} \; s_2 = \sqrt{\dfrac{n+\kappa}{2}} \end{cases} \tag{24}$$

The form of high-order UT is derived, which is an improvement to the sampling strategy of sigma points. In the framework of standard UKF, time update and measurement update of the covariance were further adjusted with the sampling strategy of sigma points. The equation (8) was modified as follows:

$$\begin{aligned} P_{k|k-1} = {} & \omega_0 \xi^{i0}_{k|k-1} (\xi^{i0}_{k|k-1})^T + \omega_1 \sum_{i1=1}^{n} \xi^{i1}_{k|k-1} \\ & (\xi^{i1}_{k|k-1})^T + \omega_2 \sum_{i2=1}^{n(n-1)/2} \xi^{i2}_{k|k-1} (\xi^{i2}_{k|k-1})^T \\ & - \hat{x}_{k|k-1} \hat{x}^T_{k|k-1} + Q_k \end{aligned} \tag{25}$$

B. OPTIMAL ADAPTIVE FACTOR BASED ON THE ESTIMATED COVARIANCE MATRIX OF PREDICTED RESIDUALS

In target tracking, it is difficult for radar to capture the real state of the target when it is strongly nonlinear, maneuvering, and moving at a high turn rate. To solve this problem, an adaptive factor was introduced to adjust the error covariance and further adjust the gain matrix to maintain the stability and robustness of the filter.

In this paper, the adaptive factor was derived from the idea of a strong tracking filter. In this method, the fading factor was introduced into the covariance matrix of state prediction, and the residual sequence is orthogonal to each other. The estimation error was adaptively adjusted to improve the tracking ability quickly. The method is robust to uncertain models and time-varying parameter systems and has good tracking for state mutations or maneuvering at high turn rate. By combining the strong tracking method with the proposed high-order UT sampling strategy, the sufficient conditions for the strong tracking filter with Gaussian constraints are given:

$$E\left\{ \left[x_k - \hat{x}_k \right] \left[x_k - \hat{x}_k \right]^T \right\} = \min \tag{26}$$

$$E\left[\varepsilon_{k+1} \varepsilon^T_k \right] = 0 \quad (k = 0, 1, 2 \cdots; j = 1, 2, \cdots) \tag{27}$$

where $\varepsilon_k = z_k + \hat{z}_{k|k-1}$. Equation (26) points out that the filtering algorithm has the minimum variance under Gaussian constraints and equation (27) requires that the residuals at different time points be orthogonal to each other. If the performance of the filtering algorithm satisfies the two conditions, it can be considered to have a strong tracking ability and optimal estimation performance. However, in the practical system, the state estimation of the filter deviates from the real value due to the mismatch of the model, resulting in a non-orthogonal output residual sequence. To maintain a good tracking ability, we introduced the fading factor into the prediction of the state error covariance matrix. The error covariance and gain matrix are adjusted online, and the covariance matrix is expanded by λ_k times. By increasing the proportion of observed data in the state estimation of the system, the forced residuals remain orthogonal to each other, and this ensures the tracking ability of the filter.

Through the implementation of high-order UT sampling method, equation (25) is modified to:

$$\begin{aligned} P^*_{k|k-1} = \lambda_k(&\omega_0\xi^{i0}_{k|k-1}(\xi^{i0}_{k|k-1})^T + \omega_1\sum_{i1=1}^{n} \\ &\xi^{i1}_{k|k-1}(\xi^{i1}_{k|k-1})^T + \omega_2\sum_{i2=1}^{n(n-1)/2} \\ &\xi^{i2}_{k|k-1}(\xi^{i2}_{k|k-1})^T - \hat{x}_{k|k-1}\hat{x}^T_{k|k-1}) + Q_k \end{aligned} \tag{28}$$

where $P^*_{k|k-1}$ represents the modified state one-step prediction covariance matrix.

From the system equation and measurement equation, the estimation error and prediction error are defined by:

$$\begin{cases} \tilde{x}_k = x_k - \hat{x}_k \\ \tilde{x}_{k-1} = x_{k-1} - \hat{x}_{k-1} \end{cases} \tag{29}$$

$$\tilde{x}_{k|k-1} = x_k - \hat{x}_{k|k-1} = F_k\tilde{x}_{k-1} + w_{k-1} \tag{30}$$

From the definition of the innovation vector, we obtain:

$$\begin{aligned} \varepsilon_k &= z_k - \hat{z}_{k|k-1} = H_k\tilde{x}_{k|k-1} + v_k \\ &= H_k\left[F_k\tilde{x}_{k-1} + w_{k-1}\right] + v_k \end{aligned} \tag{31}$$

Without loss of generality:

$$\varepsilon_{k+j} = H_{k+j}\left[F_{k+j}\tilde{x}_{k+j-1} + w_{k+j-1}\right] + v_{k+j} \tag{32}$$

where $F_k = \frac{\partial f_k(x_k)}{\partial x_k}\,|_{x_k=\hat{x}_{k-1}}$ and $H_k = \frac{\partial h_k(x_k)}{\partial x_k}\,|_{x_k=\hat{x}_{k|k-1}}$, F_k and H_k refers to the Jacobian matrix f_k and h_k and can be solved in the way of the second-order moment or higher order Taylor series expansion [55].

The covariance matrix of the predicted residual vector in EKF framework can be expressed as [56]:

$$\begin{aligned} P^{zz}_{k|k-1} &= E[z_k - \hat{z}_{k|k-1}][z_k - \hat{z}_{k|k-1}]^T \\ &= H_kP^*_{k|k-1}H^T_k + R_k \end{aligned} \tag{33}$$

$$P^{xz}_{k|k-1} = E[x_k - \hat{x}_{k|k-1}][z_k - \hat{z}_{k|k-1}]^T = P^*_{k|k-1}H^T_k \tag{34}$$

Let:

$$\begin{aligned} \eta_{k,j} &= E[\varepsilon_{k+j}\varepsilon^T_k] \\ &= E[H_{k+j}(F_{k+j}\tilde{x}_{k+j-1} + w_{k+j-1}) + v_{k+j}] \\ &\quad \times [H_k(F_k\tilde{x}_{k-1} + w_{k-1}) + v_k]^T \\ &= H_{k+j}F_{k+j}(\prod_{i=k+1}^{k+j-1}(I - K_iH_i)F_i)(P^{xz}_{k|k-1} - K_k\eta_0) \end{aligned} \tag{35}$$

where η_0 is the innovation covariance matrix of the actual output of the UKF algorithm. Let $\eta_{k,j} = 0$, then $(P^{xz}_{k|k-1} - K_k\eta_0) = 0$. Through calculations and arrangements, we see:

$$P^{xz}_{k|k-1}(I - (P^{zz}_{k|k-1})^{-1}\eta_0) = 0 \tag{36}$$

$$P^*_{k|k-1}H^T_k(I - (H_kP^*_{k|k-1}H^T_k + R_k)^{-1}\eta_0) = 0 \tag{37}$$

$$H_kP^*_{k|k-1}H^T_k = \eta_0 - R_k \tag{38}$$

The modified covariance is brought in:

$$\begin{aligned} H_k\{\lambda_k(&\omega_0\xi^{i0}_{k|k-1}(\xi^{i0}_{k|k-1})^T) \\ &+ \omega_1\sum_{i1=1}^{n}\xi^{i1}_{k|k-1}(\xi^{i1}_{k|k-1})^T) \\ &+ \omega_2\sum_{i2=1}^{n(n-1)/2}\xi^{i2}_{k|k-1}(\xi^{i2}_{k|k-1})^T) - \hat{x}_{k|k-1} \\ &\hat{x}^T_{k|k-1} + Q_k\}H^T_k = \eta_0 - R_k \end{aligned} \tag{39}$$

$$\begin{aligned} H_k\{\lambda_k(&\omega_0\xi^{i0}_{k|k-1}(\xi^{i0}_{k|k-1})^T) \\ &+ \omega_1\sum_{i1=1}^{n}\xi^{i1}_{k|k-1}(\xi^{i1}_{k|k-1})^T) \\ &+ \omega_2\sum_{i2=1}^{n(n-1)/2}\xi^{i2}_{k|k-1}(\xi^{i2}_{k|k-1})^T) - \hat{x}_{k|k-1} \\ &\hat{x}^T_{k|k-1}\}H^T_k = \eta_0 - R_k - H_kQ_kH^T_k \end{aligned} \tag{40}$$

$$\eta_k = \begin{cases} \varepsilon_1\varepsilon^T_1, & k = 1 \\ \dfrac{\rho\eta_{k-1} + \varepsilon_k\varepsilon^T_k}{1+\rho}, & k \geq 2 \end{cases} \tag{41}$$

where ρ denotes the fading factor and whose $\rho = 0.95$.

$$\begin{aligned} \lambda_k = \mathrm{tr}(&\eta_k - R_k - H_kQ_kH^T_k)/\mathrm{tr}(H_k\{(\omega_0\xi^{i0}_{k|k-1} \\ &(\xi^{i0}_{k|k-1})^T) + \omega_1\sum_{i1=1}^{n}\xi^{i1}_{k|k-1}(\xi^{i1}_{k|k-1})^T) \\ &+ \omega_2\sum_{i2=1}^{n(n-1)/2}\xi^{i2}_{k|k-1}(\xi^{i2}_{k|k-1})^T) - \hat{x}_{k|k-1}\hat{x}^T_{k|k-1}\}H^T_k) \end{aligned} \tag{42}$$

It should be noted that the λ_k in equation (42) may be less than 1. To avoid this situation and ensure the stability of the whole filtering process, the adaptive fading factor can be further chosen as:

$$\lambda_k = \max(1, \lambda_k) \tag{43}$$

For λ_k, the fading factor can take effect, therefore, the fading factor remains the same sensitivity to state mutation and stationary.

C. DISCUSSION ON THE STABILITY OF ALGORITHM

Stability is one of the key indicators of practicability. The accuracy of the proposed high-order UKF depends largely on the high-order UT strategy. Therefore, the stability of the algorithm can only be guaranteed by ensuring the stability of the high-order UT strategy. In addition, the equality constraints of equations (26), (27) and (43) are satisfied in the process of solving the adaptive factor, and the global optimization can be satisfied in model mismatch. In view of integration, the UT is also considered as a high dimensional integral method. When the high-order method is adopted, all the weights corresponding to the sigma points are positive, so this algorithm is feasible. Therefore, the sum of the absolute values of the weights is used as the technical index of the numerical stability of the algorithm. By deducing the above equations, it is found that the sigma points are completely symmetric. If $\sum \mid \omega_i \mid = 1$, the numerical integration is completely stable. If $\sum \mid \omega_i \mid \gg 1$, the introduction of large rounding errors will lead to numerical instability [9]. Therefore, when $\sum \mid \omega_i \mid \gg 0 (i = 0, 1, 2)$, satisfying $\sum \mid \omega_i \mid = 1$ invariably holds, the higher-order UT is completely stable. To make the sigma points of high-order UT match the information of high-order moment of a random function of Gaussian distribution, the stability cost function of high-order UT transform is constructed [47].

$$J_{(s_i,\omega_i)} = 2\omega_1 s_1^6 + 4(n-1)\omega_2 s_2^6 - 15 \tag{44}$$

With the cost function, the minimization problem for equation (44) is equivalent to: $J_{(s_i,\omega_i)} = 0$. The transformation is essentially de-biased and consistent. The sigma points and weights distribution satisfy the stability cost function of equation (44). So, to capture the high-order moment information of Gaussian random function and improve the accuracy of UT. s_1, ω_1, s_2 and ω_2 in equations (19), (20), and (24) are introduced into $J_{(s_i,\omega_i)}$ to obtain new cost function:

$$G_{(n,\kappa)} = (n-1)\kappa^2 + \left(2n^2 - 14n\right)\kappa + n^3 - 13n^2 + 60n - 60 \tag{45}$$

Let the cost function $G_{(n,\kappa)} = 0$, the necessary and sufficient condition for satisfaction is: $\triangle = -96n^2 + 480n - 240 \geq 0$, and thus, we have can be $2 \leq n \leq 4$, it is shown that the optimal free parameters exist only in 2-4 Dimensional state spaces.

Then only 1-4 Dimensional state spaces were analyzed and verified:

In a 1-Dimensional state, $n = 1$ is substituted into equations (18), (19), (20), and (45), respectively. Although the weights corresponding to all the sigma points taken are all positive, but equation (17) has no analytical solution, so there is no optimal free parameter selection in a 1-Dimensional state.

In a 2-Dimensional state, $n = 2$ is substituted into equations (18), (19), (20), and (45), and we get $\kappa = 0.835$ and $\kappa = 19.165$, respectively. The weights corresponding to all the sigma points taken are all positive. From the point of view of numerical stability, $\kappa = 0.835$ is selected.

In a 3-Dimensional state, $n = 3$ is substituted into equations (18), (19), (20), and (45), and we get $\kappa = 1.417$ and $\kappa = 10.583$, respectively. Similarly, the weights corresponding to all sigma points are all positive. From the point of view of numerical stability, $\kappa = 1.417$ is selected.

In the 4-Dimensional state, $n = 4$ is special. Only the free parameter $\kappa = 2$ can satisfy the weights corresponding to the sigma points, which are all positive. The following is a description of the special cases.

D. DETAILED ALGORITHM FOLLOWS

We summarized the implementation of the improved AHUKF algorithm as follows:

1) The initial value is given by equation (3) and the state vector x_{k-1} is assumed from $x_{k-1} \sim N(x_{k-1}; \hat{x}_{k-1}, P_{k-1})$.

$$\hat{x}_0 = E[x_0] \quad P_0 = E\left[\tilde{x}_0 \tilde{x}_0^T\right] \tag{46}$$

2) Determine the system state dimension, and select the optimal free parameter κ.

Time update:

3) Estimate covariance matrix P_{k-1} of the state vector by Cholesky decomposition:

$$P_{k-1} = S_{k-1} S_{k-1}^T \tag{47}$$

4) High-order sigma points and corresponding weights construction and by given in equations (18), (19) and (20).

5) Compute the propagated high-order sigma points $\xi_{k|k-1}^i$:

$$\begin{cases} \xi_{k|k-1}^{i0} = f(\xi_{k|k-1}^{i0}) \\ \xi_{k|k-1}^{i1} = f(\xi_{k|k-1}^{i1}) \\ \xi_{k|k-1}^{i2} = f(\xi_{k|k-1}^{i2}) \end{cases} \tag{48}$$

6) Compute the predicted state $\hat{x}_{k|k-1}$:

$$\hat{x}_{k|k-1} = \omega_0 \xi_{k|k-1}^{i0} + \omega_1 \sum_{i1=1}^{n} \xi_{k|k-1}^{i1} + \omega_2 \sum_{i2=1}^{n(n-1)/2} \xi_{k|k-1}^{i2} \tag{49}$$

7) Compute the predicted error covariance $P_{k|k-1}$:

$$P_{k|k-1} = \omega_0 \xi_{k|k-1}^{i0} (\xi_{k|k-1}^{i0})^T + \omega_1 \sum_{i1=1}^{n} \xi_{k|k-1}^{i1} (\xi_{k|k-1}^{i1})^T + \omega_2 \sum_{i2=1}^{n(n-1)/2} \xi_{k|k-1}^{i2} (\xi_{k|k-1}^{i2})^T - \hat{x}_{k|k-1} \hat{x}_{k|k-1}^T + Q_k \tag{50}$$

8) Compute the adaptive factor λ_k, and bring into the state error covariance matrix $P_{k|k-1}$ given in equations (41), (42), and (43).

$$P^*_{k|k-1} = \lambda_k(\omega_0\xi^{i0}_{k|k-1}(\xi^{i0}_{k|k-1})^T + \omega_1\sum_{i1=1}^{n}\xi^{i1}_{k|k-1}(\xi^{i1}_{k|k-1})^T + \omega_2\sum_{i2=1}^{n(n-1)/2}\xi^{i2}_{k|k-1}(\xi^{i2}_{k|k-1})^T - \hat{x}_{k|k-1}\hat{x}^T_{k|k-1}) + Q_k \quad (51)$$

Measurement-update:

9) Estimate the predictive covariance matrix $P^*_{k|k-1}$ of the state vector by Cholesky decomposition:

$$P^*_{k|k-1} = S^*_{k|k-1}S^{*T}_{k|k-1} \quad (52)$$

10) High-order sigma points and corresponding weights construction and by given in equations (18), (19), and (20).

11) Compute the propagated high-order sigma points $\xi'^i_{k|k-1}$:

$$\begin{cases}\xi'^{i0}_{k|k-1} = h(\xi'^{i0}_{k|k-1})\\ \xi'^{i1}_{k|k-1} = h(\xi'^{i1}_{k|k-1})\\ \xi'^{i2}_{k|k-1} = h(\xi'^{i2}_{k|k-1})\end{cases} \quad (53)$$

12) Compute the predicted measurement $\hat{z}_{k|k-1}$:

$$\hat{z}_{k|k-1} = \omega_0\xi'^{i0}_{k|k-1} + \omega_1\sum_{i1=1}^{n}\xi'^{i1}_{k|k-1} + \omega_2\sum_{i2=1}^{n(n-1)/2}\xi'^{i2}_{k|k-1} \quad (54)$$

13) Compute the innovation covariance matrix and cross-covariance matrix:

$$P^{xz}_{k|k-1} = \omega_0\xi^{i0}_{k|k-1}(\xi'^{i0}_{k|k-1})^T + \omega_1\sum_{i1=1}^{n}\xi^{i1}_{k|k-1}(\xi'^{i1}_{k|k-1})^T + \omega_2\sum_{i2=1}^{n(n-1)/2}\xi^{i2}_{k|k-1}(\xi'^{i2}_{k|k-1})^T - \hat{x}_{k|k-1}\hat{z}^T_{k|k-1} \quad (55)$$

$$P^{zz}_{k|k-1} = \omega_0\xi'^{i0}_{k|k-1}(\xi'^{i0}_{k|k-1})^T + \omega_1\sum_{i1=1}^{n}\xi'^{i1}_{k|k-1}(\xi'^{i1}_{k|k-1})^T + \omega_2\sum_{i2=1}^{n(n-1)/2}\xi'^{i2}_{k|k-1}(\xi'^{i2}_{k|k-1})^T - \hat{z}_{k|k-1}\hat{z}^T_{k|k-1} + R_k \quad (56)$$

14) Estimate the updated state, the Kalman gain and the error covariance:

$$K_k = P^{xz}_{k|k-1}(P^{zz}_{k|k-1})^{-1} \quad (57)$$

$$\hat{x}_{k|k} = \hat{x}_{k|k-1} + K_k(z_k - \hat{z}_{k|k-1}) \quad (58)$$

$$P_{k|k} = P^*_{k|k-1} - K_kP^{zz}_{k|k-1}K^T_k \quad (59)$$

IV. SIMULATION ANALYSIS

In this part, we simulated and verified the different target tracking models. In order to verify the reliability and stability of the algorithm, we use the same model as reference [54] for verification. The simulation experiment run on a platform of an Inter (R) Core (TM) i3-7100 (2.4 GHz) CPU and MATLAB 2010a. Different methods were compared. Method 1: classical UKF algorithm (UKF) $\kappa = 3 - n$, Method 2: based on the principle of the orthogonal UKF algorithm (AUKF), Method 3: standard CKF algorithm (CKF), Method 4: UKF based on high-order UT sampling strategy (HUKF), and Method 5: adaptive high-order UKF (AHUKF). To compare the performances of the proposed filtering algorithm AHUKF and other algorithms, the root mean square errors (RMSEs), the averaged RMSEs (ARMSEs), and the averaged absolute value of biases (AAVBs) of position and velocity are chosen as performance metrics. The RMSE, ARMSE, and AAVB of the position are respectively defined as follows [35], [57]:

$$RMSE_{pos}(k) = \sqrt{\frac{1}{M}\sum_{s=1}^{M}\left(\left(x^s_k - \hat{x}^s_k\right)^2 + \left(y^s_k - \hat{y}^s_k\right)^2\right)} \quad (60)$$

$$ARMSE_{pos} = \frac{1}{N}\sum_{k=1}^{N}RMSE \quad (61)$$

$$AAVB_{pos} = \frac{1}{M}\left|x^s_k - \hat{x}^s_k\right|_X \quad (62)$$

where M and N are the total number of Monte Carlo runs and the simulation time, respectively. x^s_k, y^s_k and $\hat{x}^s_k$, $\hat{y}^s_k$ are the real and estimated positions of the Monte Carlo simulation at the sth run. Similar to the RMSE and ARMSE in position, we can also formulate the RMSE and ARMSE in velocity. $|\cdot|$ is the absolute value operation, subscript represents relative to X coordinates, the coordinates relative to Y are similar to the representation of X.

In this experiment, a large system model mismatch strategy was used in Scenario 1 to apply it to single target tracking. The maneuvering target tracking model is adopted in Scenario 2 and a small sampling interval and low turn rate, large sampling interval, and high turn rate, large sampling interval and low turn rate are used to verify the effectiveness of the proposed algorithm, respectively.

Scenario 1: A single observation station with a state vector is used to track the target and the radar position is determined to be known [54], [58], [59]. The target is moving according to the motion model of continuous white noise.

$$x_k = Fx_{k-1} + Gw_{k-1} \quad (63)$$

$$F = \begin{bmatrix}\Lambda & 0_{2\times2}\\ 0_{2\times2} & \Lambda\end{bmatrix} \quad \Lambda = \begin{bmatrix}1 & \Delta t\\ \Delta t & 1\end{bmatrix}$$

$$G = \begin{bmatrix}\Gamma & 0_{2\times1}\\ 0_{2\times1} & \Gamma\end{bmatrix} \quad \Gamma = \begin{bmatrix}0.5\Delta t^2 & \Delta t\end{bmatrix}^T \quad (64)$$

where $x_k = [\varsigma_k\ \dot{\varsigma}_k\ \eta_k\ \dot{\eta}_k]^T$, ς_k, η_k and $\dot{\varsigma}_k$, $\dot{\eta}_k$ represent the position and velocity of the Cartesian coordinates,

TABLE 1. ARMSEs and running times of the different algorithms.

Algorithms	ARMSE	Max-Error	Single step running time(s)
UKF	3.742193	19.640295	0.000326
CKF	3.742055	19.640512	0.000348
AUKF	3.504636	19.566758	0.000365
HUKF	1.059423	20.535593	0.001251
AHUKF	0.729735	20.865153	0.001289

respectively. F and G denote the state transition matrix and the noise drive matrix, respectively. The parameter $\triangle t$=1 s denotes the sampling interval, $0_{2\times x}$ denotes the 2D null matrix and $[\cdot]^T$ is the transpose operation. The target is observed by a range sensor mounted on the control platform of the radar observation station, and the position is fixed. The measurement model is given by the following equation:

$$z_k = \sqrt{(\varsigma_k - X_{\text{radar}})^2 - (\eta_k - Y_{\text{radar}})^2} + v_k \tag{65}$$

where (X_{randr}, Y_{randr}) denotes position of the radar observation station, z_k is the distance of the target measured by the radar at time k.

$$\begin{cases} w_k \sim N(0, Q) \\ v_k \sim N(0, R) \end{cases} \tag{66}$$

where w_k and v_k denote the process noise and measurement noise, respectively. $N(0, \sum)$ denotes zero mean Gaussian white noise variance is $\sum$. where $Q = 1e-4 * \text{diag}([0.5\ 1])$ and $R = 10$. The position of the radar station is fixed on the coordinate system platform (200m 300m) and the target track is located in the same plane as the radar.

In this simulation, UKF, CKF, AUKF, HUKF, and AHUKF are selected for comparison. Parameter selection: $\kappa = 3 - n$. In the AUKF and AHUKF, the forgetting factor $\rho = 0.95$, the free parameter κ of AHUKF chooses the optimal parameter proposed in this paper. The target initial state and covariance are set as follows: $x_0 = [-150\ 2\ 250\ 20]^T$ and $P_0 = \text{diag}[1\ 1\ 1\ 1]$, respectively. The sampling time is 60 s and the total number of Monte Carlo runs is 100. The target gives a larger state mutation in the 31 s flight, $x_{31} = [15, 15, 15, 15]^T$. In Figs. 3-5 show the RMSEs and AAVBs of the position of the proposed filtering algorithm and other filtering algorithms, respectively. Table 1 shows the one-step running time and ARMSE of each filter, as well as the maximum error. Fig. 3 clearly shows that the RMSEs of the proposed algorithm are smaller than that of other filter algorithms. In addition, it can be seen from Table 1 that the proposed algorithm has better estimation accuracy and performance than the existing algorithms, although the running time of the proposed algorithm is higher than that of other algorithms, it still satisfies the engineering requirements.

It can be seen from Fig. 3 and Table 1 that when the target is in steady flight, the nonlinear radar ranging scheme is used and the accuracy of the algorithm is better than that of other algorithms. Especially after 10 s, the peak error and convergence rate of the algorithm are much smaller than those of the other algorithms. However, given a large mutation at 31 s, the algorithm proposed in this paper reaches the maximum peak (Max-Error), however, the next second will converge quickly. When compared with the other algorithms, HUKF is accurate than other algorithms but is still not as accurate as the algorithm proposed in this paper. To clearly illustrate the superiority of this algorithm, the error curves are shown in Figs. 4 and 5, respectively. It is not difficult to

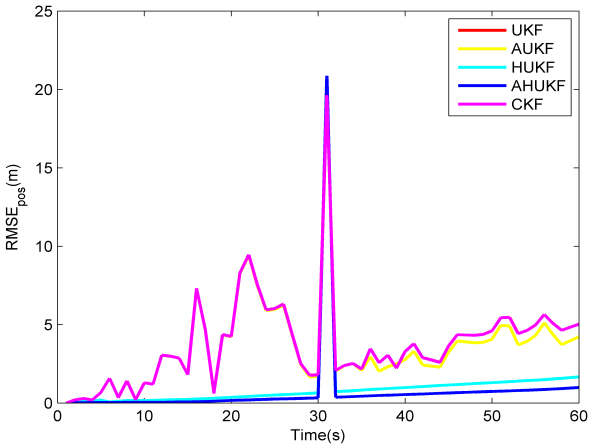

FIGURE 3. RMSEs of the different algorithms.

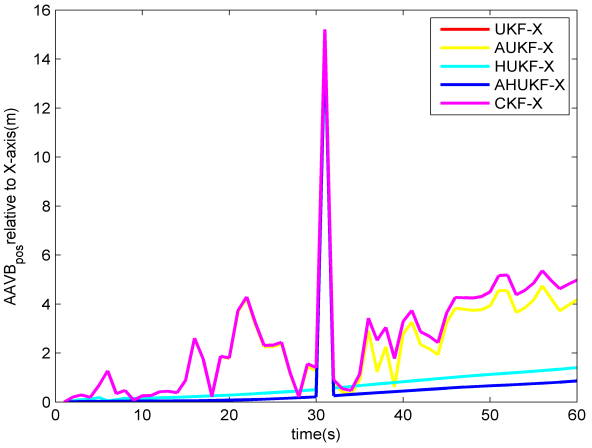

FIGURE 4. AAVBs of the X coordinates of the different algorithms.

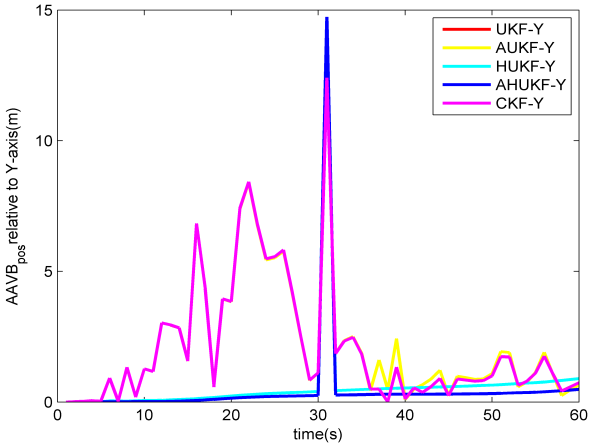

FIGURE 5. AAVBs of the Y coordinates of the different algorithms.

see that the error (AAVB) of this algorithm is lower than that of other algorithms.

It can be seen from Table 1 that the accuracy of the new algorithm proposed in this paper is 80% higher than that of UKF and CKF, and 79.17% higher than that of AUKF. In addition, when compared with the HUKF algorithm, the accuracy of the new algorithm is increased by 31.12%. The estimated trajectory of the proposed filter is closer to the real trajectory. Although the running time has increased, we mainly emphasize stability, reliability and convergence rate.

In this scenario, a large system mutation was given, and the proposed AHUKF can deal with the estimation error caused by state mutation. The high-order UT sampling strategy was used to capture the high-order moment information under nonlinear conditions, and the simulation results were also convincing.

Scenario 2: To further verify the superior the performance of proposed methods, which is applied to an agile target tracking with time-varying turn rate. This model is widely used to verify the performance of the nonlinear filter [54], [60], [61]. The computational complexity and nonlinear intensity of Scenario 2 are both higher than that of Scenario 1, and apply different sampling interval and turn rate verify the high-order moment capture capability and adaptive tracking ability of this algorithm.

Case 1: The state space model is represented as follows:

$$x_k = \begin{bmatrix} 1 & \frac{\sin \Omega\Delta T}{\Omega} & 0 & \frac{\cos \Omega\Delta T - 1}{\Omega} \\ 0 & \cos \Omega\Delta T & 0 & -\sin \Omega\Delta T \\ 0 & \frac{1-\cos \Omega\Delta T}{\Omega} & 1 & \frac{\sin \Omega\Delta T}{\Omega} \\ 0 & \sin \Omega\Delta T & 0 & \cos \Omega\Delta T \end{bmatrix} x_{k-1} + w_{k-1} \tag{67}$$

where the state is $x_k = [\varsigma_k \ \dot{\varsigma}_k \ \eta_k \ \dot{\eta}_k]^T$, ς_k and η_k denote the positions, $\dot{\varsigma}_k$ and $\dot{\eta}_k$ the denote velocities in the x and y directions, respectively. $\Omega = -1.145°s^{-1}$ denotes the constant turn rate. The process noise is $\omega \sim N(0, Q)$ with $Q =$ diag[0.1 0.01 0.1 0.01] and ΔT=1 s denotes the sampling interval.

The measurement model is represented as follows:

$$z_k = \begin{bmatrix} r_k \\ \theta_k \end{bmatrix} = \begin{bmatrix} \sqrt{x_k^2 + y_k^2} \\ \text{atan}\,2\,(y_k, x_k) \end{bmatrix} + v_k \tag{68}$$

where z_k is the measurement of the radar at moment k, arctan 2 denotes the four quadrant tangent function. It is assumed that the radar measurement range is r and azimuth is θ. The measurement noise is $v_k \sim N(0, R)$ with $R =$ diag$[\sigma_r^2 \ \sigma_\theta^2]$, where $\sigma_r = 100$m and $\sigma_\theta = 100$mrad.

The initial state is given by:

$$x_0 = \left[100\text{m}\ 20\text{ms}^{-1}\ 500\text{m}\ 30\text{ms}^{-1}\right]^T \tag{69}$$

The associated initial state covariance is given by:

$$P_{0|0} = \left[100\text{m}^2\ 10\text{m}^2\text{s}^{-2}\ 100\text{m}^2\ 10\text{m}^2\text{s}^{-2}\right] \tag{70}$$

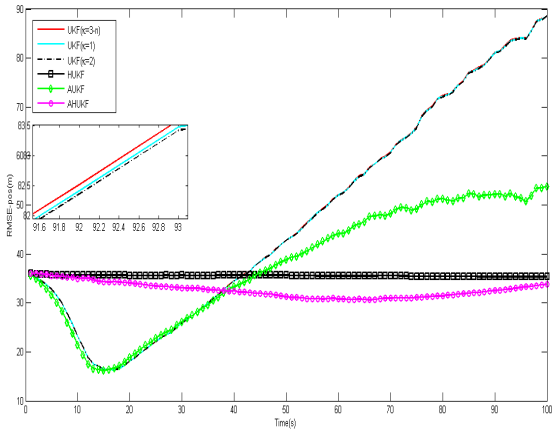

FIGURE 6. RMSEs of the position in 100 independent Monte Carlo runs for small sampling interval and low turn rate.

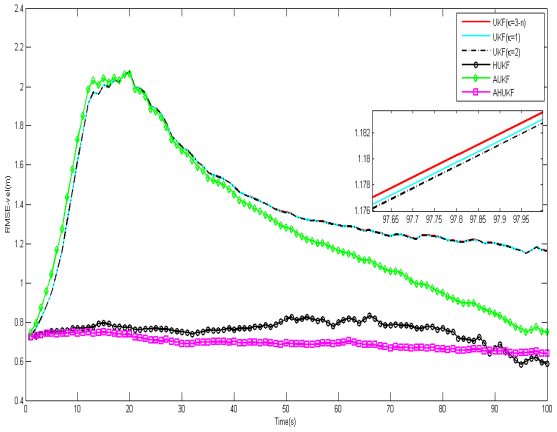

FIGURE 7. RMSEs of the velocity in 100 independent Monte Carlo runs for small sampling interval. and low turn rate.

In each run, the initial state estimation $\hat{x}_{0|0}$, was randomly selected from $N(\hat{x}_{0|0}; x_0, P_{0|0})$, and all filters were initialized under the same conditions. To compare the performance of the filter, the RMSE of the position and velocity was chosen as the performance metric, and 100 independent Monte Carlo runs were performed. To verify the importance of the derived adaptive adjustment factor and the selection of UKF free parameters, UKF ($\kappa = 3 - n$), UKF ($\kappa = 1$), UKF ($\kappa = 2$), HUKF and UKF with adaptive adjustment factor (AUKF) were compared with the algorithm proposed in this paper. The RMSE of the different filter positions and velocities are shown in Figs. 6 and 7, respectively. The ARMSE of the different filter positions and velocities and the one-step running time are shown in Table 2. It can be seen from Figs. 6 and 7 that in the proposed algorithm, the RMSE is lower than the other filters. Within 20 s, the RMSE stability of the UKF and AUKF was not ideal and had fluctuations, and then the error increased sharply. Although the error of the AUKF was reduced after 60 s, it was still larger than the HUKF and AUKF. For the HUKF and AHUKF with lower error, the error of the AHUKF was always smaller than that of the HUKF. Table 2 shows that the average tracking

TABLE 2. RMSEs of different filters position and velocity with small sampling interval and low turn rate.

Algorithms	ARMSE-Pos	ARMSE-Vel	Single step running time(s)
UKF($\kappa = 3 - n$)	47.393712	1.410311	0.000422
UKF($\kappa = 1$)	47.340996	1.409736	0.000410
UKF($\kappa = 2$)	47.314402	1.409444	0.000408
HUKF	35.559213	0.753476	0.000920
AUKF	37.889986	1.290512	0.000452
AHUKF	32.614032	0.692156	0.000960

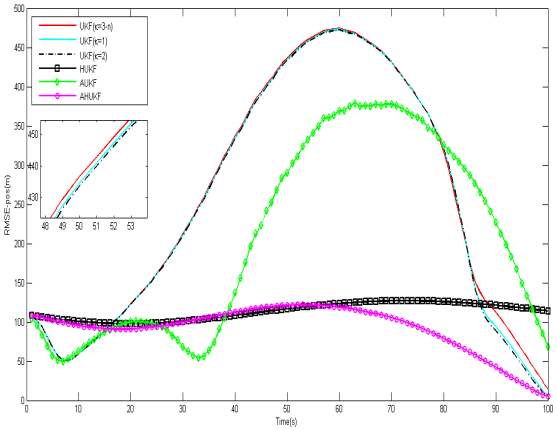

FIGURE 8. RMSEs of the position in 100 independent Monte Carlo runs for large sampling interval and low turn rate.

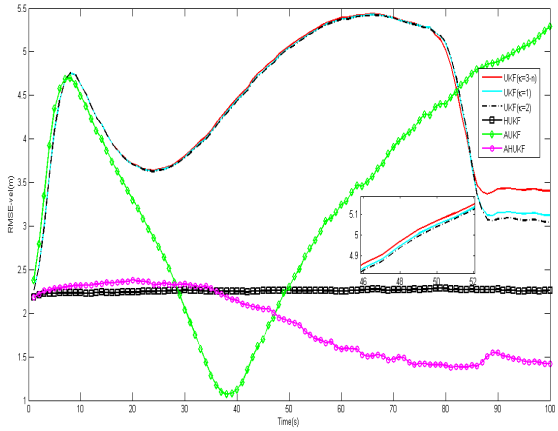

FIGURE 9. RMSEs of the velocity in 100 independent Monte Carlo runs for large sampling interval and low turn rate.

accuracy of this algorithm is also better than that of the other algorithms. The position accuracy of the proposed algorithm was 31 % higher than that of the UKF ($\kappa = 3 - n$), UKF ($\kappa = 1$),UKF ($\kappa = 2$), 8% and 14% higher than that of the HUKF and AUKF, respectively.

Case 2: To verify the robustness of the proposed algorithm, we deliberately increased the sampling interval and kept the other parameters unchanged. Sampling interval ΔT=3 s, the algorithm was further tested in Case 2. Figs. 8 and 9 show the position and velocity of the RMSEs, respectively. Table 3 shows the different filter position and velocity of ARMSE and one-step running time. From Figs. 8 and 9, due to the mismatch of higher-order moment information

TABLE 3. ARMSEs of different filters position and velocity with large sampling interval and low turn rate.

Algorithms	ARMSE-Pos	ARMSE-Vel	Single step running time(s)
UKF($\kappa = 3 - n$)	254.516599	4.378633	0.000415
UKF($\kappa = 1$)	251.811686	4.337135	0.000406
UKF($\kappa = 2$)	250.844819	4.324421	0.000404
HUKF	113.282259	2.256368	0.000917
AUKF	205.041944	3.408174	0.000449
AHUKF	91.852067	1.881525	0.000959

TABLE 4. ARMSEs of different filter position and velocity with large sampling interval and high turn rate.

Algorithms	ARMSE-Pos	ARMSE-Vel	Single step running time(s)
UKF($\kappa = 3 - n$)	78.488111	12.175480	0.000407
UKF($\kappa = 1$)	78.509154	12.178916	0.000399
UKF($\kappa = 2$)	78.519649	12.180629	0.000401
HUKF	107.170158	16.839124	0.000901
AUKF	73.782270	11.403088	0.000443
AHUKF	58.480713	8.115988	0.000948

in the state estimation, the UKF (including different free parameters) and AUKF contain a large jump. For the AUKF, it is difficult to adjust the estimation of covariance in a weak maneuvering state, which can result in the gain difficult to reach the required value, but it is still superior to the method of the UKF (including different free parameters). Under the condition of capturing the information of high-order moments, AHUKF adjusts the prediction error covariance effectively by using an adaptive adjustment factor, so the error accuracy is better than that of AUKF, and the robustness is very good. The proposed algorithm is superior to other algorithms in large sampling intervals. Compared with the UKF algorithm, the accuracy of the AHUKF was improved by 63.6%. Compared with the AUKF algorithm, the accuracy of AHUKF is improved by 55.2%. For HUKF, AHUKF was still a great improvement, and the accuracy of the improvement of 18.9%.

Case 3: On the basis of Case2, the simulation test was carried out again, and the maneuvering tracking test was carried out under the condition of high turn rate, where $\Omega = -9°s^{-1}$. Figs. 10 and 11 show the position and velocity of the RMSEs, respectively. Table 4 shows the error statistics of the test.

In this simulation, the superiority of the proposed algorithm can be better explained. As can be clearly seen in Figs. 10 and 11, HUKF tends to be stationary, but the error is higher than all filters. This is because the tracking information is too smooth to capture the real information, leading to the gradual deviation of the tracking trajectory, which reduces the tracking performance of the radar system, precision reduction by 45% compared with AHUKF. When compared with AUKF, under the condition of high turn rate and large sampling interval, the adaptive factor played a major role in adjusting, but it was still not better than the algorithm proposed in this paper, and compared with AHUKF, the tracking accuracy decreases by 20.7%.

In this scenario, a large sampling interval was easy to lose sampling information, and the high turn rate led to increased maneuverability of the target. AHUKF can more accurate

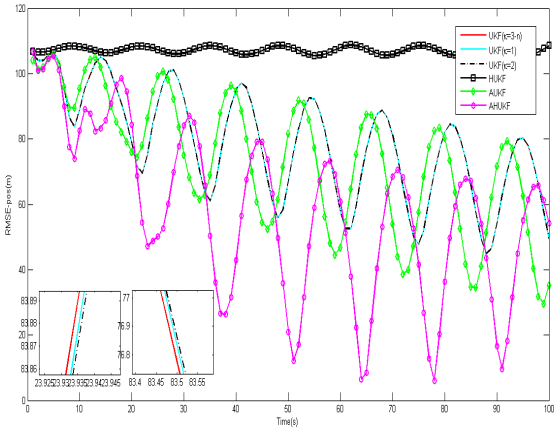

FIGURE 10. RMSEs of the position in 100 independent Monte Carlo runs for large sampling interval and high turn rate.

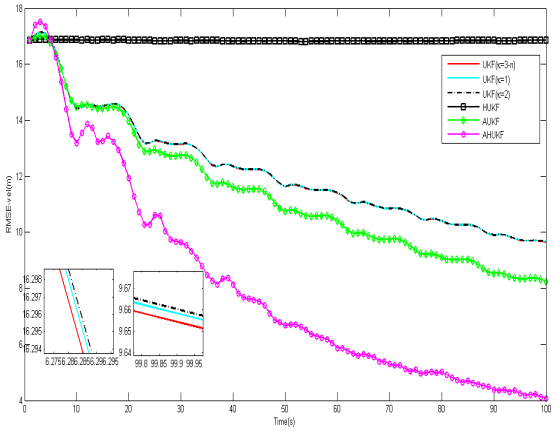

FIGURE 11. RMSEs of the velocity in 100 independent Monte Carlo runs for large sampling interval and high turn rate.

matching of the high-order moment information, reducing the error caused by the model mismatch. Thus, the proposed AHUKF had better filtering precision than the existing filtering in a target tracking application with the different sampling interval and turn rate, respectively, and can achieve the global optimal.

The above experiments and analysis demonstrated the proposed AHUKF enhances the robustness of the classical UKF and outperforms other filtering methods in accuracy under model mismatches, large sampling interval and high running rate.

V. CONCLUSION

In this paper, a new adaptive high-order unscented Kalman filter (AHUKF) was proposed by using the orthogonal principle and high-order UT sampling strategy based on an online estimation method, and it was applied to the target tracking model. For the standard UKF algorithm, only the first two moments can be captured. In this paper, a high-order UT sampling strategy with free parameters was proposed to capture the information of high-order moments and improve the estimation accuracy. The rationality of the selection of free parameters was analyzed theoretically. Based on the orthogonal principle, the adaptive factor was introduced into the prediction covariance, and the gain matrix was further adjusted, which effectively restrains the influence of strong nonlinear and maneuvering target as well as large abrupt changes on the filter. AHUKF had a good effect on different sampling intervals and different turning rates, and the effect of the dynamic model error was reduced. The experimental results show that the proposed method was robust in suppressing the uncertainty of the model and had a good ability to capture high-order moment information. The estimation accuracy was improved, the global optimization was achieved, and the stability of the whole filtering process was improved. The results show that the AHUKF algorithm had advantages over the other filtering algorithms. The computational complexity was slightly higher than the other Gaussian approximation algorithms. We believe the AHUKF would be still useful in engineering applications.

Future research on AHUKF might extend the field of nonlinear singularly perturbed complex networks [62], discrete time-delayed genetic regulatory networks under stochastic communication protocols [63], [64], and non-stationary heavy tailed noises [65], [66].

ACKNOWLEDGEMENT

The authors would like to thank coordinating editor and anonymous reviewers for very useful and constructive feedback.

REFERENCES

[1] N. Sadeghzadeh-Nokhodberiz and J. Poshtan, "Distributed interacting multiple filters for fault diagnosis of navigation sensors in a robotic system," *IEEE Trans. Syst., Man, Cybern. Syst.*, vol. 47, no. 7, pp. 1383–1393, Jul. 2017.

[2] W. Liu, P. Shi, and J.-S. Pan, "State estimation for discrete-time Markov jump linear systems with time-correlated and mode-dependent measurement noise," *Automatica*, vol. 85, no. 11, pp. 9–21, Nov. 2017.

[3] M. Gupta, S. Kumar, L. Behera, and V. K. Subramanian, "A novel vision-based tracking algorithm for a human-following mobile robot," *IEEE Trans. Syst., Man, Cybern. Syst.*, vol. 47, no. 7, pp. 1415–1427, Jul. 2017.

[4] S. Zhao, Y. S. Shmaliy, P. Shi, and C. K. Ahn, "Fusion Kalman/UFIR filter for state estimation with uncertain parameters and noise statistics," *IEEE Trans. Ind. Electron.*, vol. 64, no. 4, pp. 3075–3083, Apr. 2017.

[5] L. Wang, Z. Liu, C. L. P. Chen, Y. Zhang, S. Lee, and X. Chen, "A UKF-based predictable SVR learning controller for biped walking," *IEEE Trans. Syst., Man, Cybern. Syst.*, vol. 43, no. 6, pp. 1440–1450, Nov. 2013.

[6] Y. Huang, Y. Zhang, Z. Wu, N. Li, and J. Chambers, "A novel adaptive Kalman filter with inaccurate process and measurement noise covariance matrices," *IEEE Trans. Autom. Control*, vol. 63, no. 2, pp. 594–601, Feb. 2018.

[7] G. Hu, W. Wang, Y. Zhong, B. Gao, and C. Gu, "A new direct filtering approach to INS/GNSS integration," *Aerosp. Sci. Technol.*, vol. 77, pp. 755–764, Jun. 2018.

[8] B. Gao, G. Hu, S. Gao, Y. Zhong, and C. Gu, "Multi-sensor optimal data fusion for INS/GNSS/CNS integration based on unscented Kalman filter," *Int. J. Control Autom. Syst.*, vol. 16, no. 1, pp. 129–140, Feb. 2018.

[9] Y. Wu, D. Hu, M. Wu, and X. Hu, "A numerical-integration perspective on Gaussian filters," *IEEE Trans. Signal Process.*, vol. 54, no. 8, pp. 2910–2921, Aug. 2006.

[10] B. D. O. Anderson and J. B. Moore, *Optimal Filtering*. Englewood Cliffs, NJ, USA: Prentice-Hall, 1979.

[11] Y. Huang, Y. Zhang, B. Xu, Z. Wu, and J. A. Chambers, "A new adaptive extended Kalman filter for cooperative localization," *IEEE Trans. Aerosp. Electron. Syst.*, vol. 54, no. 1, pp. 353–368, Feb. 2018.
[12] G. Hu, S. Gao, and Y. Zhong, "A derivative UKF for tightly coupled INS/GPS integrated navigation," *ISA Trans.*, vol. 56, pp. 135–144, May 2015.
[13] B. D. O. Anderson, J. B. Moore, and M. Eslami, "Optimal filtering," *IEEE Trans. Syst., Man, Cybern. Syst.*, vol. 12, no. 2, pp. 235–236, Mar./Apr. 1982.
[14] X. Liu, H. Qu, J. Zhao, P. Yue, and M. Wang, "Maximum correntropy unscented Kalman filter for spacecraft relative state estimation," *Sensors*, vol. 16, no. 9, pp. 1530–1546, Sep. 2016.
[15] S. Julier, J. Uhlmann, and H. F. Durrant-Whyte, "A new method for the nonlinear transformation of means and covariances in filters and estimators," *IEEE Trans. Autom. Control*, vol. 5, no. 3, pp. 477–482, Mar. 2000.
[16] S. J. Julier and J. K. Uhlmann, "Unscented filtering and nonlinear estimation," *Proc. IEEE*, vol. 92, no. 3, pp. 401–422, Mar. 2004.
[17] Y. Huang, Y. Zhang, N. Li, and J. Chambers, "Robust Student's t based nonlinear filter and smoother," *IEEE Trans. Aerosp. Electron. Syst.*, vol. 52, no. 5, pp. 2586–2596, Oct. 2016.
[18] I. Arasaratnam and S. Haykin, "Cubature Kalman filters," *IEEE Trans. Autom. Control*, vol. 54, no. 6, pp. 1254–1269, Jun. 2009.
[19] K. Ito and K. Xiong, "Gaussian filters for nonlinear filtering problems," *IEEE Trans. Autom. Control*, vol. 45, no. 5, pp. 910–927, May 2000.
[20] Z. Duan, A. Jahanzeb, G. Imran, J. Muhammad, K. Ikramullah, and A. Khurram, "Improving the tracking of subatomic particles using the unscented Kalman filter with measurement redundancy in high energy physics experiments," *IEEE Access*, vol. 7, no. 5, pp. 61728–61737, May 2019.
[21] S. Gao, G. Hu, and Y. Zhong, "Windowing and random weighting-based adaptive unscented Kalman filter," *IEEE Trans. Autom. Control*, vol. 29, no. 2, pp. 201–223, Jan. 2014.
[22] P. J. Costa and W. H. Moore, "Extended Kalman-Bucy filters for radar tracking and identification," in *Proc. IEEE Nat. Radar Conf.*, Los Angeles, CA, USA, Mar. 1991, pp. 127–131.
[23] L. Ma, Z. Wang, Q.-L. Han, and H.-K. Lam, "Variance-constrained distributed filtering for time-varying systems with multiplicative noises and deception attacks over sensor networks," *IEEE Sensors J.*, vol. 17, no. 7, pp. 2279–2288, Apr. 2017.
[24] L. Ma, Z. Wang, Q.-L. Han, and H.-K. Lam, "Envelope-constrained H_∞ filtering for nonlinear systems with quantization effects: The finite horizon case," *Automatica*, vol. 93, pp. 527–534, Jul. 2018.
[25] L. Ma, Z. Wang, H.-K. Lam, and N. Kyriakoulis, "Distributed event-based set-membership filtering for a class of nonlinear systems with sensor saturations over sensor networks," *IEEE Trans. Cybern.*, vol. 47, no. 11, pp. 3772–3783, Nov. 2017.
[26] T. Lefebvre, H. Bruyninckx, and J. De Schuller, "Comment on 'a new method for the nonlinear transformation of means and covariances in filters and estimators,'" *IEEE Trans. Autom. Control*, vol. 47, no. 8, pp. 1406–1409, Nov. 2002.
[27] J. Hou and W. Zhou, "Application of improved UPF algorithm in nonlinear non-Gauss system," in *Proc. 14th IEEE Int. Conf. Signal Process. (ICSP)*, Aug. 2018, pp. 84–89.
[28] J. Loxam and T. Drummond, "Student-t mixture filter for robust, real-time visual tracking," in *Proc. 10th Eur. Conf. Comput. Vis. (ECCE)*, 2008, pp. 372–385.
[29] Y. Huang and Y. Zhang, "Robust Student's t-based stochastic cubature filter for nonlinear systems with heavy-tailed process and measurement noises," *IEEE Access*, vol. 5, pp. 7964–7974, 2017.
[30] Z. Gao, D. Mu, S. Gao, Y. Zhong, and C. Gu, "Adaptive unscented Kalman filter based on maximum posterior and random weighting," *Aerosp. Sci. Technol.*, vol. 71, pp. 12–24, Dec. 2017.
[31] L. Li, D. Yu, Y. Xia, and H. Yang, "Event-triggered UKF for nonlinear dynamic systems with packet dropout," *Int. J. Robust Nonlinear Control*, vol. 27, no. 18, pp. 4208–4226, Dec. 2017.
[32] M. Xiao, Y. Zhang, and H. Fu, "Three-stage unscented Kalman filter for state and fault estimation of nonlinear system with unknown input," *J. Franklin Inst.*, vol. 354, no. 18, pp. 8421–8443, Dec. 2017.
[33] X. Cheng, M. Bi, and H. Liu, "A new prediction unscented Kalman filter based on robust model and its application," in *Proc. 3rd IEEE Inf. Technol. Mechatronics Eng. Conf. (ITOEC)*, Oct. 2017, pp. 895–903.
[34] L. Chang, B. Hu, G. Chang, and A. Li, "Huber-based novel robust unscented Kalman filter," *IET Sci. Meas. Technol.*, vol. 6, no. 6, pp. 502–509, Nov. 2012.
[35] Y. Huang, Y. Zhang, Z. Wu, N. Li, and J. Chambers, "A novel robust Student'st-based Kalman filter," *IEEE Trans. Aerosp. Electron. Syst.*, vol. 53, no. 3, pp. 1545–1554, Jun. 2017.
[36] X. Wang, N. Cui, and J. Guo, "Huber-based unscented filtering and its application to vision-based relative navigation," *IET Radar Sonar Navigation*, vol. 4, no. 1, pp. 134–141, Feb. 2010.
[37] F. El-Hawary and Y. Jing, "Robust regression-based EKF for tracking underwater targets," *IEEE J. Ocean. Eng.*, vol. 20, no. 1, pp. 31–41, Jan. 1995.
[38] Y. Wang, S. Sun, and L. Li, "Adaptively robust unscented Kalman filter for tracking a maneuvering vehicle," *J. Guid. Control Dyn.*, vol. 37, no. 5, pp. 1696–1701, Jun. 2014.
[39] Y. Huang and Y. Zhang, "A new process uncertainty robust Student's t based Kalman filter for SINS/GPS integration," *IEEE Access*, vol. 5, pp. 14391–14404, 2017.
[40] L. Chang, B. Hu, G. Chang, and A. Li, "Marginalised iterated unscented Kalman filter," *IET Control Theory Appl.*, vol. 6, no. 6, pp. 847–854, Apr. 2012.
[41] L. Chang, B. Hu, A. Li, and F. Qin, "Strapdown inertial navigation system alignment based on marginalised unscented Kalman filter," *IET Sci., Meas. Technol.*, vol. 7, no. 2, pp. 128–138, Mar. 2013.
[42] K. Xiong, H. Zhang, and L. Liu, "Adaptive robust extended Kalman filter for nonlinear stochastic systems," *IET Control Theory Appl.*, vol. 2, no. 3, pp. 239–250, Mar. 2008.
[43] H. Zhang, J. Xie, J. Ge, W. Lu, and B. Zong, "Adaptive strong tracking square-root cubature Kalman filter for maneuvering aircraft tracking," *IEEE Access*, vol. 6, pp. 10052–10061, 2018.
[44] H. Zhang, J. Xie, J. Ge, W. Lu, and B. Liu, "Strong tracking SCKF based on adaptive CS model for manoeuvring aircraft tracking," *IET Radar, Sonar Navigat.*, vol. 12, no. 7, pp. 742–749, Jul. 2018.
[45] S. Zhao, Y. S. Shmaliy, C. K. Ahn, and F. Liu, "Adaptive-horizon iterative UFIR filtering algorithm with applications," *IEEE Trans. Ind. Electron.*, vol. 65, no. 8, pp. 6393–6402, Aug. 2008.
[46] Q. Wang, "The theory and application research of adaptive-robust UKF for satellite integrated navigation system," Huazhong Univ. Sci. Technol., Wuhan, China, 2010, pp. 68–72.
[47] S. J. Julier and J. K. Uhlmann, "A consistent, debiased method for converting between polar and cartesian coordinate systems," in *Proc. AeroSense, 11th Int. Symp. Aerosp./Defense Sens., Simulation Contr.*, Orlando, FL, USA, Jun. 1997, pp. 110–121.
[48] J. Rezaie and J. Eidsvik, "A skewed unscented Kalman filter," *Int. J. Control*, vol. 89, no. 12, pp. 2572–2583, Apr. 2016.
[49] K. Ponomareva, P. Date, and Z. Wang, "A new unscented Kalman filter with higher order moment-matching," in *Proc. 19th Int. Symp. Math. Theory Netw. Syst.*, Jun. 2010, pp. 1609–1613.
[50] B. Gao, G. Hu, S. Gao, Y. Zhong, and C. Gu, "Multi-sensor optimal data fusion based on the adaptive fading unscented Kalman filter," *sensors*, vol. 18, no. 2, p. 488, Feb. 2018.
[51] B. Gao, S. Gao, Y. Zhong, G. Hu, and C. Gu, "Interacting multiple model estimation-based adaptive robust unscented Kalman filter," *Int. J. Control, Automat. Syst.*, vol. 15, no. 5, pp. 2013–2025, Oct. 2017.
[52] B. Jia and M. Xin, "Sparse-grid quadrature H_∞ filter for discrete-time systems with uncertain noise statistics," *IEEE Trans. Aerosp. Electron. Syst.*, vol. 49, no. 3, pp. 1626–1636, Aug. 2013.
[53] M.-J. Yu, "INS/GPS integration system using adaptive filter for estimating measurement noise variance," *IEEE Trans. Aerosp. Electron. Syst.*, vol. 48, no. 2, pp. 1786–1792, Apr. 2012.
[54] X. R. Li and V. P. Jilkov, "Survey of maneuvering target tracking. Part I. Dynamic models," *IEEE Trans. Aerosp. Electron. Syst.*, vol. 39, no. 4, pp. 1333–1364, Oct. 2003.
[55] W. Zhou, J. Hou, L. Liu, T. Sun, and J. Liu, "Design and simulation of the integrated navigation system based on extended Kalman filter," *Open Phys.*, vol. 15, no. 1, pp. 182–187, Jan. 2017.
[56] W. Zhou and J. Hou, "A new adaptive robust unscented Kalman filter for improving the accuracy of target tracking," *IEEE Access*, vol. 7, pp. 77476–77489, 2019.
[57] Y. Huang, Y. Zhang, P. Shi, Z. Wu, J. Qian, and J. A. Chambers, "Robust Kalman filters based on Gaussian scale mixture distributions with application to target tracking," *IEEE Trans. Syst., Man, Cybern. Syst.*, to be published.

[58] Y. Huang and Y. Zhang, "Design of high-degree Student's t-based cubature filters," *Circuits Syst. Signal Process.*, vol. 37, no. 5, pp. 2206–2225, May 2018.
[59] Y. Huang, Y. Zhang, N. Li, and L. Zhao, "Design of sigma-point Kalman filter with recursive updated measurement," *Circuits Syst. Signal Process.*, vol. 35, no. 5, pp. 1767–1782, May 2016.
[60] B.-T. Vo, B.-N. Vo, and A. Cantoni, "Bayesian filtering with random finite set observations," *IEEE Trans. Signal Process.*, vol. 56, no. 4, pp. 1313–1326, Apr. 2008.
[61] J. Liu, Z. Wang, and M. Xu, "A Kalman estimation based rao-blackwellized particle filtering for radar tracking," *IEEE Access*, vol. 5, pp. 8162–8174, 2017.
[62] X. Wan, Z. Wang, M. Wu, and X. Liu, "H_∞ state estimation for discrete-time nonlinear singularly perturbed complex networks under the round-robin protocol," *IEEE Trans. Neural Netw. Learn. Syst.*, vol. 30, no. 2, pp. 415–426, Jul. 2018.
[63] X. Wan, Z. Wang, Q.-L. Han, and M. Wu, "Finite-time H_∞ state estimation for discrete time-delayed genetic regulatory networks under stochastic communication protocols," *IEEE Trans. Circuits Syst. I, Reg. Papers*, vol. 65, no. 10, pp. 3481–3491, Oct. 2018.
[64] X. Wan, Z. Wang, M. Wu, and X. Liu, "State estimation for discrete time-delayed genetic regulatory networks with stochastic noises under the round-robin protocols," *IEEE Trans. Nanobiosci.*, vol. 17, no. 2, pp. 145–154, Apr. 2018.
[65] Y. Huang, Y. Zhang, Y. Zhao, and J. A. Chambers, "A novel robust Gaussian–Student's t mixture distribution based Kalman filter," *IEEE Trans. Signal Process.*, vol. 67, no. 13, pp. 3606–3620, Jul. 2019.
[66] Y. Huang, Y. Zhang, B. Xu, Z. Wu, and J. Chambers, "A new outlier-robust Student's t based Gaussian approximate filter for cooperative localization," *IEEE/ASME Trans. Mechatronics*, vol. 22, no. 5, pp. 2380–2386, Oct. 2017.

WEIDONG ZHOU received the bachelor's and master's degrees from the Harbin Institute of Technology, Harbin, China, in 1988 and 1991, respectively, and the Ph.D. degree from the College of Automation, Harbin Engineering University, Harbin, in 2016. In October 2004, he visited Baco Company, Belgium, and participated in many international academic conferences. He is currently a Professor of navigation, guidance, and control with Harbin Engineering University. His current research interests include signal processing, information fusion, and their applications in navigation technology, such as inertial navigation and integrated navigation.

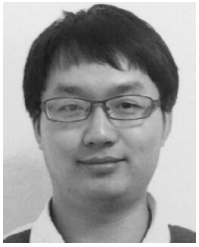

JIAXIN HOU received the B.S. degree from the Department of Automation, Northeast Petroleum University, Daqing, China, in 2006, He is currently pursuing the Ph.D. degree in control science and engineering with Harbin Engineering University, Harbin, China. His current research interests include signal processing, information fusion, and their applications in navigation technology, such as inertial navigation and integrated navigation.